Materials Sciences and Applications, 2026, 17(7), 189-214
https://www.scirp.org/journal/msa
ISSN Online: 2153-1188
ISSN Print: 2153-117X

Study on Vibration Performance of Carbon Fiber/Aluminum Alloy Shaft

Wenzhuo Dai[1], Min Huang[2], Zhonghua Huang[1*], Peng Yan[1]

[1]Hunan Institute of Engineering, Xiangtan, China
[2]South China University of Technology, Guangzhou, China
Email: csu707@163.com

How to cite this paper: Dai, W.Z., Huang, M., Huang, Z.H. and Yan, P. (2026) Study on Vibration Performance of Carbon Fiber/Aluminum Alloy Shaft. *Materials Sciences and Applications*, **17**, 189-214.
https://doi.org/10.4236/msa.2026.177013

Received: June 4, 2026
Accepted: July 28, 2026
Published: July 31, 2026

Abstract

High-speed power systems impose higher requirements on the vibration performance of shafts. High-damping composite materials are beneficial to improving the vibration performance of shafts. In this paper, a carbon fiber/aluminum alloy shaft is taken as the research object. The prediction models of the first-order damping loss factor and natural frequency are fitted by the response surface methodology, and the influence of the interaction of various parameters on the vibration reduction performance of the shaft is analyzed. Then, the multi-objective optimization using genetic algorithm obtains the parameter combination closest to the ideal solution (maximizing both the first-order damping loss factor and natural frequency): the ply angle is 24˚, the layup mode is symmetric, the adhesive layer thickness is 0.2 mm, and the adhesive layer coverage ratio is 90%. Specimens of Al/CFRP shaft and aluminum alloy shaft are fabricated. Through modal experimental analysis, the simulation and optimization results are verified experimentally. The research shows that the finite element model and prediction model have high accuracy. Compared with the aluminum alloy shaft, the optimized Al/CFRP shaft increases the first-order modal frequency and damping loss factor by 7.69% and 283.30%, respectively.

Keywords

Composite Materials, Shaft, Vibration, Damping

1. Introduction

The shaft is the core component for mechanical power transmission, and its dynamic characteristics have a significant influence on the stability, reliability and working efficiency of the whole machine [1]. Metal shafts are widely used due to their excellent strength, stiffness and mature manufacturing technology. However, such materials generally exhibit low damping performance. The low damping characteristic makes it difficult to dissipate vibration energy effectively during shaft operation, especially when crossing the critical speed or operating under a wide speed range, which easily induces severe resonance. This not only accelerates the wear and fatigue of connecting parts such as bearings, but also may even lead to shaft fracture and failure in serious cases, threatening the safe operation of equipment [2] [3]. Improving the high-speed operation stability and vibration performance of shafts has become an urgent problem to be solved in the design of power system shafting.

To address the problem of insufficient damping in metal shafts, carbon fiber reinforced composites can be adopted to improve the vibration performance of shafts. Kim *et al.* [4] found that composite shafts possess higher natural frequencies than metal shafts, and analyzed the effects of parameters such as lay-up angle and aspect ratio on their natural frequencies. Gubran *et al.* [5] focused on the lay-up sequence of carbon fibers to investigate its influence on the natural frequency of carbon fiber shafts. Sino *et al.* [6] analyzed the effects of lay-up sequence, ply orientation, transverse shear and other factors on the natural frequency and critical instability value of shafts. Mutasher *et al.* [7] studied the static and dynamic characteristics of shafts with different fiber types, lay-up sequences, winding angles and layer numbers. Sarvestani *et al.* [8] investigated the effect of shear loading on the stress distribution of composite tubes. Xu Zhaotang *et al.* [9] took a new composite helicopter shaft as the research object, analyzed the primary resonance problem, and proposed improving the damping performance to ensure stable operation. The above studies show that shafts based on carbon fiber composites have obvious advantages in weight and moment of inertia, and their performance is closely related to structural parameters and manufacturing processes.

However, the relatively high manufacturing cost of composite shafts remains a bottleneck for their large-scale engineering application. To achieve high stiffness and high damping simultaneously, composite/metal hybrid structures have become a promising design approach. Accordingly, this paper proposes a high-damping hybrid shaft structure composed of carbon fiber and aluminum alloy. It combines high-damping carbon fiber with low-cost, high-toughness aluminum, improving the dynamic characteristics of the structure while controlling cost. Sun *et al.* [10] experimentally investigated the energy absorption characteristics of aluminum tubes, CFRP tubes, and Al/CFRP hybrid tubes. The results show that the energy absorption capacity of Al/CFRP hybrid tubes is significantly superior to that of single-material tubes. On this basis, using the established numerical simulation method, they studied the effects of different lengths, thicknesses, and fiber lay-up angles on the performance of hybrid tubes. Kabir *et al.* [11] established a finite element model of carbon fiber-reinforced concrete-filled steel tubular columns using ABAQUS. The results show that the addition of carbon fiber sheets can significantly improve the strength and stiffness of members, but the growth rate of strength decreases with an increase in the number of carbon fiber layers. The above studies systematically verify that metal/fiber hybrid structures exhibit excellent comprehensive performance from multiple perspectives such as mechanical properties.

The mechanical properties of metal/fiber hybrid structures are affected not only by the parameters of the ply structure, but also by the structural parameters of the adhesive layer. Shao Jiaru *et al.* [12] conducted experiments on single adhesive joints of composite materials with different lay-up modes and thicknesses. The results show that the degradation shape and failure load of the adhesive layer are closely related to the ply angles on both sides of the adhesive layer. Farin *et al.* [13] discussed the effects of lay-up sequence, adhesive materials, surface treatment and other factors on the bonding strength of carbon fiber reinforced composites. Kupski *et al.* [14] tested single-lap joints with four lay-up modes and analyzed the influence of lay-up mode on the static tensile failure of joints. Akash *et al.* [15] used a two-component epoxy adhesive to bond fiber adherends in single-lap configuration, and studied the joint strength of single-lap adhesive joints under linear variation of adhesive layer thickness.

The structural parameters of carbon fiber composites and the characteristic parameters of bonding interfaces are closely related to their service performance. The research on the vibration characteristics of high-damping carbon fiber/aluminum alloy hybrid shafts is still insufficient. To reveal the relationship between shaft structural parameters and vibration damping control, it is necessary to establish a vibration performance model for carbon fiber/aluminum alloy shafts. This paper focuses on the vibration performance design of the shaft. The optimal design scheme is obtained by using response surface methodology and genetic algorithm, and its accuracy is verified through shaft modal tests.

2. Heoretical Analysis on Dynamics of Carbon Fiber Composites

2.1. Theoretical Analysis on Stiffness of Carbon Fiber Composites

According to the basic theoretical framework of composite mechanics, when an anisotropic material system undergoes deformation within the range of small deformation, the constitutive relationship between the internal stress field and strain field can be accurately described by the generalized Hooke's law:

$$\begin{bmatrix} \sigma_1 \\ \sigma_2 \\ \sigma_3 \\ \tau_{23} \\ \tau_{31} \\ \tau_{12} \end{bmatrix} = \begin{bmatrix} C_{11} & C_{12} & C_{13} & C_{14} & C_{15} & C_{16} \\ C_{21} & C_{22} & C_{23} & C_{24} & C_{25} & C_{26} \\ C_{31} & C_{32} & C_{33} & C_{34} & C_{35} & C_{36} \\ C_{41} & C_{42} & C_{43} & C_{44} & C_{45} & C_{46} \\ C_{51} & C_{52} & C_{53} & C_{54} & C_{55} & C_{56} \\ C_{61} & C_{62} & C_{63} & C_{64} & C_{65} & C_{66} \end{bmatrix} \begin{bmatrix} \varepsilon_1 \\ \varepsilon_2 \\ \varepsilon_3 \\ \gamma_{23} \\ \gamma_{31} \\ \gamma_{12} \end{bmatrix} \tag{1}$$

In the formula: from left to right are the stress component matrix $[\sigma]$, stiffness matrix $[C]$, and strain component matrix of the composite material $[\varepsilon]$, respectively. $\sigma_i\ (i=1,2,3)$ is the stress component in the *i*-direction; $\tau_{ij}\ (i,j=1,2,3)$ is the shear stress in the *i*-*j* plane; $\varepsilon_i\ (i=1,2,3)$ is the normal strain in the *i*-direction; $\gamma_{ij}\left(i,j=1,2,3\right)$ is the shear strain in the *i-j* plane; C_{ij} ; is the stiffness coefficient, From the analysis of material mechanical properties, it can be seen that in a three-dimensional fully elastic body, $C_{ij}=C_{ji}$ ($i,j=1,2,3,4,5,6$). The stiffness matrix has the key characteristic of symmetry. For a fiber composite material system, its material coordinate system is generally defined as follows: the 1-axis corresponds to the principal fiber direction; the 2-axis denotes the in-plane transverse direction perpendicular to the fibers; and the 3-axis represents the thickness direction normal to the fiber orientation. With the establishment of this coordinate system, the original expression can be simplified:

$$\sigma=C\varepsilon \tag{2}$$

The compliance matrix is used to represent the relationship between strain and stress, namely:

$$\begin{bmatrix}\varepsilon_1\\ \varepsilon_2\\ \varepsilon_3\\ \gamma_{23}\\ \gamma_{31}\\ \gamma_{12}\end{bmatrix}=\begin{bmatrix}S_{11}&S_{12}&S_{13}&S_{14}&S_{15}&S_{16}\\ S_{21}&S_{22}&S_{23}&S_{24}&S_{25}&S_{26}\\ S_{31}&S_{32}&S_{33}&S_{34}&S_{35}&S_{36}\\ S_{41}&S_{42}&S_{43}&S_{44}&S_{45}&S_{46}\\ S_{51}&S_{52}&S_{53}&S_{54}&S_{55}&S_{56}\\ S_{61}&S_{62}&S_{63}&S_{64}&S_{65}&S_{66}\end{bmatrix}\begin{bmatrix}\sigma_1\\ \sigma_2\\ \sigma_3\\ \tau_{23}\\ \tau_{31}\\ \tau_{12}\end{bmatrix} \tag{3}$$

Thus the above equation can be simplified as:

$$\varepsilon=S\sigma \tag{4}$$

where: S is the compliance matrix of the structure, and S_{ij} denotes the stiffness coefficient.

Carbon Fiber Reinforced Polymer (CFRP), as a typical fiber-reinforced resin matrix composite, exhibits significant orthotropic properties. This material system has three mutually perpendicular planes of elastic symmetry, corresponding to the 2-3 plane, 3-1 plane, and 1-2 plane, respectively. According to this symmetry, the stress-strain relationship in its constitutive equation can be effectively simplified:

$$\begin{bmatrix}\sigma_1\\ \sigma_2\\ \sigma_3\\ \tau_{23}\\ \tau_{31}\\ \tau_{12}\end{bmatrix}=\begin{bmatrix}C_{11}&C_{12}&C_{13}&0&0&0\\ C_{21}&C_{22}&C_{23}&0&0&0\\ C_{31}&C_{32}&C_{33}&0&0&0\\ 0&0&0&C_{44}&0&0\\ 0&0&0&0&C_{55}&0\\ 0&0&0&0&0&C_{66}\end{bmatrix}\begin{bmatrix}\varepsilon_1\\ \varepsilon_2\\ \varepsilon_3\\ \gamma_{23}\\ \gamma_{31}\\ \gamma_{12}\end{bmatrix} \tag{5}$$

Therefore, having $C_{22}=C_{33}$, $C_{12}=C_{13}$, $C_{55}=C_{66}$, meanwhile, it is further derived based on the equality of strain potential energy density:

$$C_{44}=\frac{1}{2}\left(C_{22}-C_{23}\right) \tag{6}$$

In this matrix, there are only C_{11}, C_{22}, C_{12}, C_{23}, C_{44}, C_{55} independent stiffness coefficients. In practical applications, the relationship between stress and strain is usually expressed in terms of engineering elastic constants for convenience in testing.

$$\begin{cases} C_{11} = \dfrac{1-\nu_{23}\nu_{32}}{E_2 E_3 \Delta}; C_{22} = C_{33} = \dfrac{1-\nu_{13}\nu_{31}}{E_1 E_3 \Delta} \\ C_{23} = \dfrac{\nu_{32}+\nu_{12}\nu_{31}}{E_1 E_3 \Delta} \\ C_{44} = G_{23} \\ C_{55} = G_{12} \end{cases} \tag{7}$$

$$\Delta = \frac{1-\nu_{12}\nu_{21}-\nu_{23}\nu_{32}-\nu_{31}\nu_{13}-2\nu_{21}\nu_{32}\nu_{13}}{E_1 E_2 E_3} \tag{8}$$

where: E_1, E_2, E_3 are the elastic moduli in different directions; E_1, E_2, E_3 are the shear moduli in different directions; ν_{12}, ν_{21}, ν_{23}, ν_{32}, ν_{13}, ν_{31} are the Poisson's ratios in different directions. The relationships among them are as follows:

$$\begin{cases} \dfrac{\nu_{12}}{E_1} = \dfrac{\nu_{21}}{E_2} \\ \dfrac{\nu_{13}}{E_1} = \dfrac{\nu_{31}}{E_3} \\ \dfrac{\nu_{23}}{E_2} = \dfrac{\nu_{31}}{E_3} \end{cases} \tag{9}$$

2.2. Stiffness Theory of Composite Laminates

Composite components generally adopt a laminated structure composed of unidirectional materials stacked at various ply angles. According to the basic assumptions of Classical Laminated Plate Theory, the dimension in the thickness direction (*i.e.*, direction 3) is much smaller than that in the in-plane directions (directions 1 and 2). Therefore, it can be approximated as $\sigma_3 = 0$, $\tau_{23} = \tau_{31} = 0$. At this time, the internal stress-strain relationship can be simplified as:

$$\begin{bmatrix} \sigma_1 \\ \sigma_2 \\ \tau_{12} \end{bmatrix} = \begin{bmatrix} Q_{11} & Q_{12} & 0 \\ Q_{12} & Q_{22} & 0 \\ 0 & 0 & Q_{66} \end{bmatrix} \begin{bmatrix} \varepsilon_1 \\ \varepsilon_2 \\ \gamma_{12} \end{bmatrix} \tag{10}$$

Based on the in-plane elastic properties of a single lamina in the principal material coordinate system, each component of its stiffness matrix can be characterized by engineering elastic constants. This matrix is adopted as a key parameter in the above theoretical calculation model:

$$\begin{cases} Q_{11} = \dfrac{E_1}{(1-\nu_{12}\nu_{21})} \\ Q_{12} = \dfrac{\nu_{12}E_2}{(1-\nu_{12}\nu_{21})} \\ Q_{22} = \dfrac{E_2}{(1-\nu_{12}\nu_{21})} \\ Q_{66} = G_{12} \end{cases} \tag{11}$$

However, the above stress-strain relationship is only applicable to the special case where the material coordinate system (1-2) of a single lamina coincides exactly with the global coordinate system (x-y) of the laminate. As illustrated in Figure 1, in practical engineering applications, there exists a specific ply angle θ between the principal fiber direction of each lamina and the principal axis of the laminate. Therefore, it is necessary to transform the off-axis stresses and strains in the global coordinate system obtained from the constitutive relation to the principal material directions of each individual lamina for analysis.

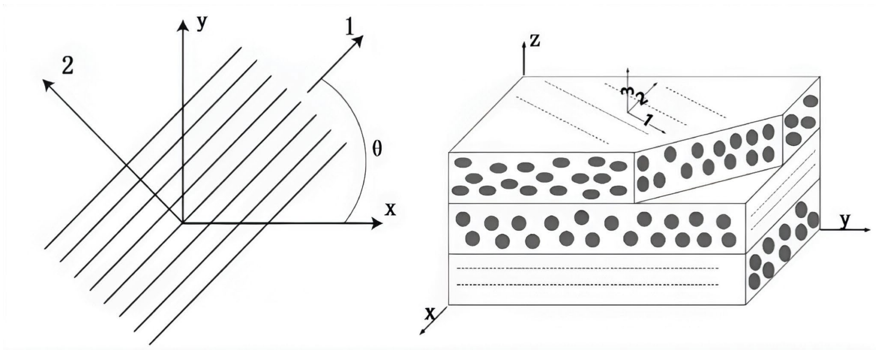

Figure 1. Angular difference between the two coordinate systems.

The relationship between the stiffness matrices in the two directions $\bar{Q}$ (off-axis direction) and Q (principal material direction) is given by:

$$\bar{Q} = T^{-1} Q \left(T^{-1}\right)^{\mathrm{T}} \tag{12}$$

where: T is the coordinate transformation matrix, whose specific elements can be expressed as:

$$T = \begin{bmatrix} \cos^2\theta & \sin^2\theta & 2\sin\theta\cos\theta \\ \sin^2\theta & \cos^2\theta & -2\sin\theta\cos\theta \\ -\sin\theta\cos\theta & \sin\theta\cos\theta & \cos^2\theta - \sin^2\theta \end{bmatrix} \tag{13}$$

Based on the deformation assumptions of laminate theory, the stress-strain relation of a single lamina in the global coordinate system can be expressed using the strain vector on the midplane and the curvature change vector of the midplane:

$$\begin{bmatrix} \sigma_x \\ \sigma_y \\ \tau_{xy} \end{bmatrix} = \begin{bmatrix} \bar{Q}_{11} & \bar{Q}_{12} & \bar{Q}_{16} \\ \bar{Q}_{12} & \bar{Q}_{22} & \bar{Q}_{26} \\ \bar{Q}_{16} & \bar{Q}_{26} & \bar{Q}_{66} \end{bmatrix} \begin{bmatrix} \varepsilon_x^0 \\ \varepsilon_y^0 \\ \gamma_{xy}^0 \end{bmatrix} \left\{ \begin{bmatrix} \varepsilon_x^0 \\ \varepsilon_y^0 \\ \gamma_{xy}^0 \end{bmatrix} + z_k \begin{bmatrix} k_x \\ k_y \\ k_{xy} \end{bmatrix} \right\} \tag{14}$$

where: ε_x^0, ε_y^0, γ_{xy}^0 represent the normal strains and shear strain on the midplane; k_x, k_y denote the bending curvatures of the midplane; k_{xy} is the twisting curvature of the midplane; z_k is the distance from the k-th lamina to the neutral surface. According to Equation (11), each stiffness coefficient of the off-axis stiffness matrix is given by:

$$\begin{cases} \bar{Q}_{11} = Q_{11}\cos^4\theta + 2\left(Q_{12} + 2Q_{66}\right)\sin^2\theta\cos^2\theta + Q_{22}\sin^4\theta \\ \bar{Q}_{12} = Q_{12}\left(\sin^4\theta + \cos^4\theta\right) + \left(Q_{11} + Q_{22} - 4Q_{66}\right)\sin^2\theta\cos^2\theta \\ \bar{Q}_{22} = Q_{11}\sin^4\theta + 2\left(Q_{12} + 2Q_{66}\right)\sin^2\theta\cos^2\theta + Q_{22}\cos^4\theta \\ \bar{Q}_{16} = \left(Q_{11} - Q_{12} - 2Q_{66}\right)\sin\theta\cos^3\theta + \left(Q_{12} - Q_{22} + 2Q_{66}\right)\sin^3\theta\cos\theta \\ \bar{Q}_{26} = \left(Q_{11} - Q_{12} - 2Q_{66}\right)\sin^3\theta\cos\theta + \left(Q_{12} - Q_{22} + 2Q_{66}\right)\sin\theta\cos^3\theta \\ \bar{Q}_{66} = \left(Q_{11} + Q_{22} - 2Q_{12} - 2Q_{66}\right)\sin^2\theta\cos^2\theta + Q_{66}\left(\sin^4\theta + \cos^4\theta\right) \end{cases} \tag{15}$$

Thus, it can be concluded that the global stiffness characteristics of composite laminated structures are mainly affected by the ply angles and stacking sequence of each individual lamina.

2.3. Calculation Procedure for Damping Ratio of Composite Materials

As can be concluded from the foregoing analysis, the key to obtaining each order damping ratio of CFRP structural components lies in accurately extracting the stress and strain distribution data of the structure under each mode shape, followed by solving relevant parameters through numerical computation. On this basis, this study adopts the Ansys finite element analysis platform and applies the Lanczos mode ex-traction algorithm to calculate multiple natural frequencies and corresponding mode shapes of the Al/CFRP transmission shaft. Afterwards, the stress and strain field data of each finite element are exported via the APDL post-processing module. Finally, a dedicated calculation program is developed in the Matlab programming environment to complete the numerical solution of damping parameters. The detailed calculation procedure is illustrated in **Figure 2**.

Partial APDL command streams are listed as follows:

```
/POST1
*CREATE,READCODE,MAC
*DO,J,1,20
ALLSEL,ALL
SET,1,J
ETABLE,EJ,SENE
SSUM
*GET,EJ_ALL,SSUM,,ITEM,EJ
*CFOPEN,EJ_ALL%J%,TXT
*VWRITE,EJ_ALL
(F20.6)
*CFCLOS
*ENDDO
*DO,J,1,20
ALLSEL,ALL
SET,1,J
*DO,I,1,4        ESEL,S,MAT,,I
```

```
ETABLE,EJI%I%,SENE
SSUM
*GET,EJI_ALL%I%,SSUM,,ITEM,EJI%I%
*ENDDO
*CFOPEN,EJI_ALL%J%,TXT
*DO,I,1,4
*VWRITE,EJI_ALL%I%
(F20.6)
*ENDDO
*CFCLOS
*ENDDO
*END
READCODE
```

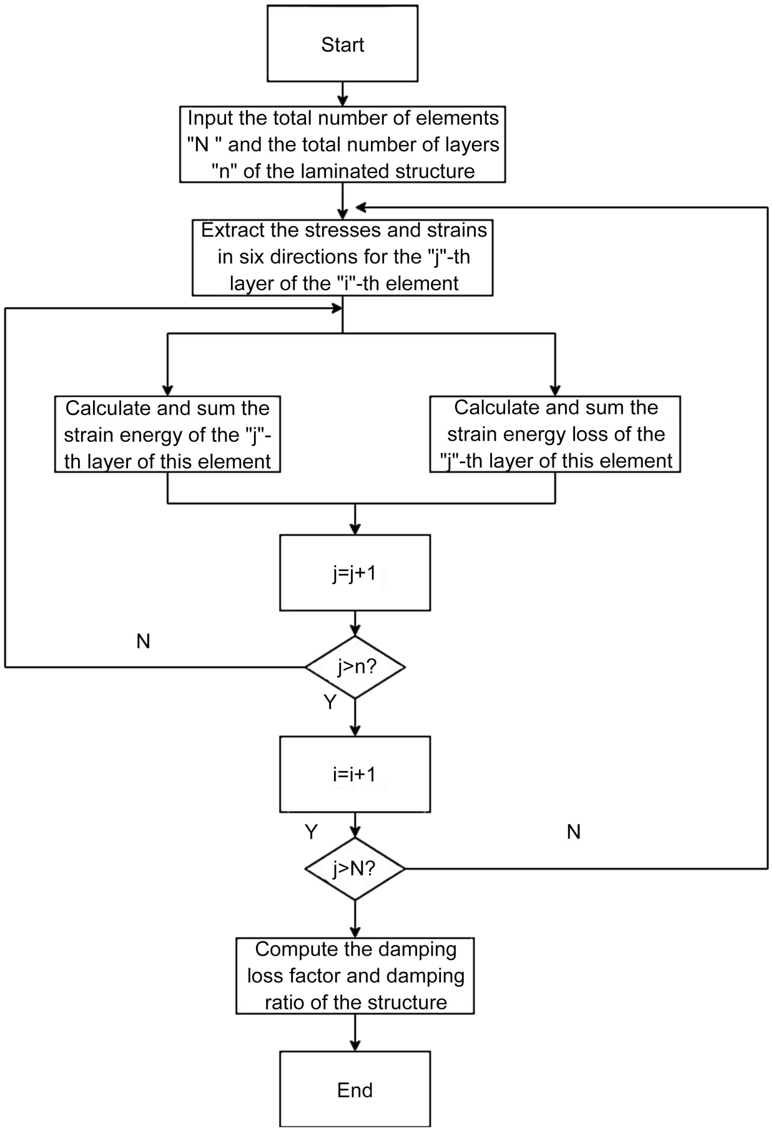

Figure 2. Flow chart of the damping ratio calculation program.

3. Construction of Prediction Model Based on Response Surface Methodology and Finite Element Simulation

3.1. Finite Element Model Construction

As shown in Figure 3, a shaft for engineering machinery has load positions at both ends, while the middle section bears torque. The modeling of the carbon fiber/aluminum alloy shaft is illustrated in Figure 4. To meet the vibration damping requirements and assembly requirements of the shaft, the dimensions of the shaft must remain unchanged.

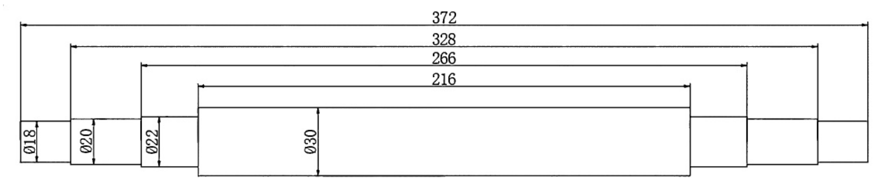

Figure 3. Flow chart of the damping ratio calculation program.

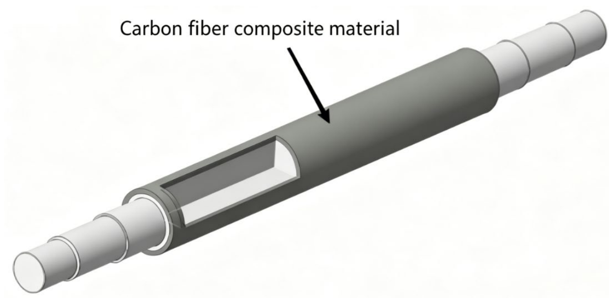

Figure 4. Modeling diagram of Al/CFRP shaft.

The carbon fiber layers are made of T300/YPH-308 unidirectional prepreg tape. The volume fractions of carbon fiber and epoxy resin are 68% and 32%, respectively. Its basic mechanical properties are: E_x = 135 GPa, E_y = 10 GPa, G_{xy} = 5.5 GPa, ν_{xy} = 0.28, ρ = 1600 kg/m^3. The specific material properties of the aluminum alloy shaft core are: E = 71 GPa, ν = 0.33, ρ = 2770 kg/m^3.

The adhesive layer is made of epoxy adhesive DP-460, whose basic mechanical parameters are as follows: E = 1.65 GPa, ν = 0.28, ρ = 1140 kg/m^3, η = 0.05%.

The ACP module in ANSYS Workbench can be used for composite material modeling and analysis. Figure 5 shows the interface for setting CFRP ply parameters. The specific operation procedure is as follows: First, select the composite material with defined material properties in the Fabric module and specify the lamina thickness of each ply. Then, set the fiber orientation angle of each ply through the Stackup module. Define the ply coordinate system direction by combining Rosettes and Oriented selection sets. Uniformly define the overall ply thickness in Modeling Groups. Convert ply data into solid geometry via the Solid Models module. Finally, couple and transfer data between ACP Pre and Mechanical Model according to the requirements of the analysis type. As shown in Figure 6, the mesh type adopted is Hex Dominant. The mesh size is 1 mm for carbon fiber layers and adhesive layers, and 3 mm for the metal shaft. The total number of elements is 203,938.

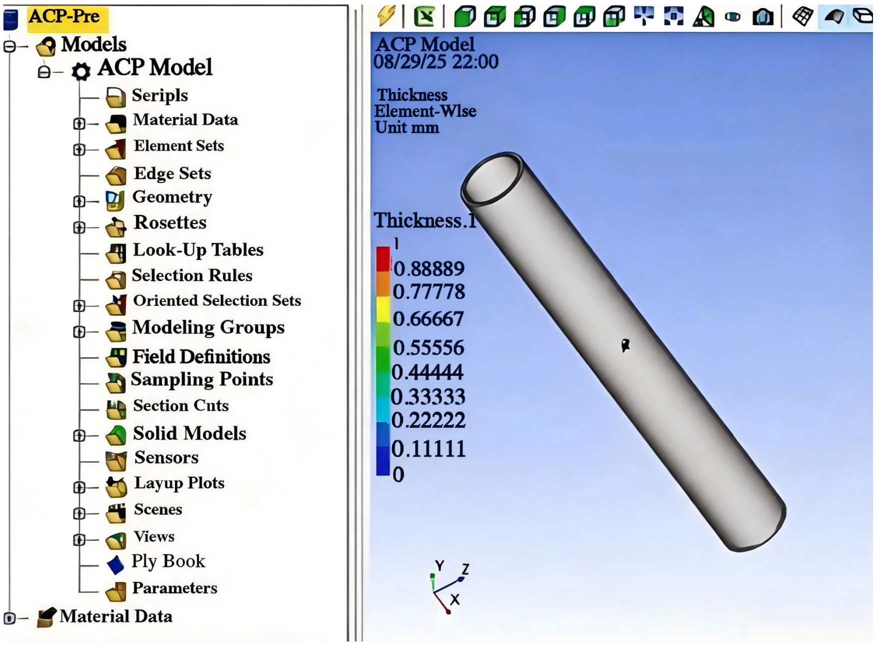

Figure 5. CFRP ply design interface.

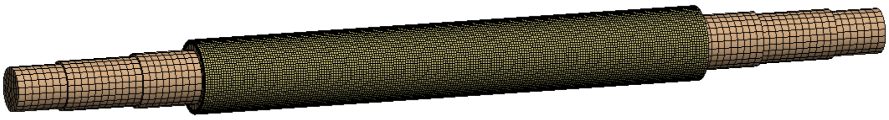

Figure 6. Finite element mesh generation.

According to the actual operating state of the transmission shaft, the boundary conditions shown in Figure 7 are applied to it with simply supported constraints. Remote displacement constraints are configured as follows: all translational displacements along the X, Y and Z directions and all rotational displacements about the X and Z axes at end A are set to zero, while the translational displacement along the Y axis is left free. At end B, all translational displacements along the Y and Z directions and all rotational displacements about the X and Z axes are set to zero, and the translational displacement along the X direction (rotation about the Y axis) is set free.

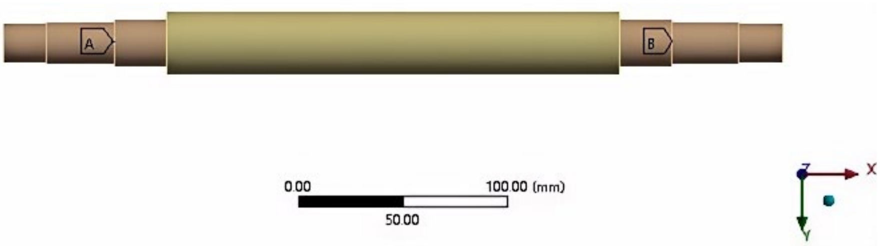

Figure 7. Schematic diagram of constraint settings.

To eliminate the interference of mesh discretization errors on the calculated modal frequencies and damping loss factors, a mesh independence verification is carried out, and the corresponding schemes and results are listed in Table 1.

Table 1. Mesh sensitivity simulation results.

No.	Mesh size of carbon fiber and adhesive layer/mm	Mesh size of shaft body/mm	1st natural frequency/Hz	Damping loss factor/%
1	2	4	847.64	0.318
2	1.5	3.5	849.27	0.331
3	1	3	850.99	0.341
4	0.5	2.5	851.16	0.343

The mesh sensitivity simulation results indicate that after refining the mesh size of carbon fiber layers and adhesive layers to 1 mm and the mesh size of the metal shaft to 3 mm, the first-order natural frequency and damping loss factor tend to stabilize with a relative error less than 1%. Considering both convergence accuracy and computational cost comprehensively, this mesh size is adopted as the uniform standard mesh in this paper.

3.2. Design of Simulation Experiments Based on Response Surface Methodology

Response Surface Methodology, also known as regression design, explores the influence laws of various experimental factors and their interactions on the target response by designing multi-factor and multi-level experimental combinations. On the basis of experimental data, an accurate mathematical regression model is established, which can effectively predict and optimize the investigated indicators [16].

In this paper, the Box-Behnken Design (BBD) principle of response surface methodology is adopted for factor design of ply angle, stacking sequence, adhesive layer thickness and laying ratio, to reveal the influence laws of different ply structures and bonding interface parameters on the damping loss factor and first-order natural frequency of the shaft, and to fit its prediction model.

It can be concluded from literature results that the shaft exhibits optimal damping performance when the ply angle is approximately 30˚, the layup sequence is symmetric, the adhesive layer thickness is 0.2 mm, and the laying proportion is 80%. The number of carbon fiber plies and the thickness of each single ply are set to be identical across different schemes of ply parameters. The levels and coding of each parameter are listed in Tables 2-5.

Table 2. Ply angle and coding.

Level	Name	Stacking Sequence B
−1	A1	15
0	A2	30
1	A3	45

Table 3. Stacking sequence and coding.

Level	Name	Stacking Sequence B
−1	B1	[θ]8
0	B2	[θ/-θ]4
1	B3	[0˚/θ/-θ/90˚]S

Table 4. Adhesive layer thickness and coding.

Level	Name	Stacking Sequence B
−1	C1	0.15
0	C2	0.20
1	C3	0.25

Table 5. Adhesive lay-up ratio and coding.

Level	Name	Stacking Sequence B
−1	D1	60
0	D2	80
1	D3	100

Since the layup sequence is a categorical variable, it cannot be input as a continuous value. Therefore, a discrete design variable z_2 is introduced, where $z_2 = 1$, 2, 3 correspond to three lamination stacking configurations [θ]8, [θ/-θ]4, [0˚/θ/-θ/90˚]S, respectively.

Std	Run	Factor 1 A: Laying angle (˚)	Factor 2 B: Stacking sequence	Factor 3 C: Bondline thickness (mm)	Factor 4 D: Rubber layer ratio (%)	Response 1 Damping factor (%)	Response 2 Natural frequency (Hz)
1	16	15	1	0.2	80		
2	1	45	1	0.2	80		
3	24	15	3	0.2	80		
4	15	45	3	0.2	80		
5	27	30	2	0.15	60		
6	22	30	2	0.25	60		
7	17	30	2	0.15	100		
8	15	30	2	0.25	100		
9	13	15	2	0.2	60		
10	2	45	2	0.2	60		
11	28	15	2	0.2	100		
12	19	45	2	0.2	100		
13	4	30	1	0.15	80		
14	29	30	3	0.15	80		
15	12	30	1	0.25	80		
16	8	30	3	0.25	80		
17	3	15	2	0.15	80		
18	9	45	2	0.15	80		
19	18	15	2	0.25	80		
20	26	45	2	0.25	80		
21	20	30	2	0.2	60		
22	11	30	3	0.2	60		
23	10	30	1	0.2	100		
24	6	30	3	0.2	100		
25	7	30	2	0.2	80		
26	5	30	2	0.2	80		
27	21	30	2	0.2	80		
28	14	30	2	0.2	80		
29	23	30	2	0.2	80		

Figure 8. Box-Behnken experimental design plan.

According to the level ranges of ply parameters and adhesive layer parameters in Tables 2-5, a four-factor, three-level experimental design was carried out, yielding 29 test points as shown in Figure 8.

3.3. Simulation Analysis of Test Methods

According to the experimental scheme shown in Figure 8, simulation analysis was carried out using ANSYS Workbench. The simulation results of 29 groups of damping loss factors obtained are listed in Table 6 and input into the design scheme of Figure 8.

Table 6. Adhesive lay-up ratio and coding.

No.	A: Ply angle/˚	B: Stacking sequence	C: Adhesive layer thickness/mm	D: Adhesive lay-up ratio/%	η: Damping loss factor/%	f: 1st natural frequency/Hz
1	15	1	0.2	80	0.34	850.99
2	45	1	0.2	80	0.24	715.73
3	15	3	0.2	80	0.47	832.02
4	45	3	0.2	80	0.41	765.78
5	30	2	0.15	60	0.35	785.69
6	30	2	0.25	60	0.38	783.33
7	30	2	0.15	100	0.55	787.13
8	30	2	0.25	100	0.55	785.75
9	15	2	0.2	60	0.45	855.06
10	45	2	0.2	60	0.28	716.91
11	15	2	0.2	100	0.55	856.45
12	45	2	0.2	100	0.5	719.4
13	30	1	0.15	80	0.15	778.78
…						
29	30	2	0.2	80	0.75	785.2

3.4. Establishment of First-Order Damping Loss Factor Prediction Model

The experimental data of damping loss factor in Table 6 were subjected to multiple regression analysis using Design-Expert software, and the prediction model of the first-order damping loss factor is obtained as follows:

$$\begin{aligned} \eta = & -6.9233 + 0.0326 z_1 + 1.3883 z_2 + 33.1333 z_3 + 0.0551 z_4 \\ & + 0.0000667 z_1 z_2 + 0.01 z_1 z_3 + 0.0001 z_1 z_4 - 0.006 z_2 z_4 - 0.0075 z_3 z_4 \\ & - 0.0007986 z_1^2 - 0.2133 z_2^2 - 81.3333 z_3^2 - 0.000243 z_4^2 \end{aligned} \quad (16)$$

where: z_1, z_2, z_3 and z_4 represent the ply angle, stacking sequence, adhesive layer thickness and adhesive lay-up ratio, respectively.

3.5. Regression Diagnostics of the First-Order Damping Loss Factor Prediction Model

Analysis of Variance (ANOVA) is a statistical technique that examines the statistical significance of the regression model and evaluates the model reliability by comparing the ratio of the regression mean square to the residual mean square (F-statistic). By decomposing the total variation of data into components derived from different factors, this method can effectively verify the fitting effect of the model. The analysis results can identify the significant main factors, secondary factors and interaction effects between various factors on the dependent variable [17]. **Table 7** shows the ANOVA of the prediction model for damping loss factor.

Table 7. ANOVA of the prediction model for damping loss factor.

Source	Sum of Squares	Degrees of Freedom	Mean Square	F-value	P-value
Model	0.8994	14	0.0642	13.96	<0.0001
z_1 : Ply angle	0.0420	1	0.0420	9.13	0.0092
z_2 : Stacking sequence	0.0675	1	0.0675	14.66	0.0018
z_3 : Adhesive layer thickness	0.0027	1	0.0027	0.05866	0.4565
z_4 : Adhesive lay-up ratio	0.1610	1	0.1610	34.98	<0.0001
z_1z_2	0.0004	1	0.0004	0.0869	0.7725
z_1z_3	0.0002	1	0.0002	0.0489	0.8282
z_1z_4	0.0036	1	0.0036	0.7821	0.3914
z_2z_3	0.0000	1	0.0000	0.0000	1.0000
z_2z_4	0.0576	1	0.0576	12.51	0.0033
z_3z_4	0.0002	1	0.0002	0.0489	0.8282
z_1^2	0.2092	1	0.2092	45.45	<0.0001
z_1^2	0.2952	1	0.2952	64.13	<0.0001
z_1^2	0.2682	1	0.2682	58.26	<0.0001
z_1^2	0.0611	1	0.0611	13.28	0.0027
Residual	0.0644	14	0.0046	—	——
Lack of Fit	0.0644	10	0.0064	—	—
Error	0.0000	4	0.0000	—	—
Total	0.9638	28	—	—	—

As can be seen from **Table 7**, the P-value of the model is much less than 0.05, indicating that the model is extremely significant and has strong prediction ability. Among them, the significance levels of ply angle, stacking sequence and adhesive lay-up ratio are $P < 0.01$, so these three factors all have significant effects on damping performance. In the parameter interactions, the interaction between stacking sequence and adhesive lay-up ratio has a significance level of $P = 0.003 <$

0.05, indicating that this interaction term has a significant influence on damping performance. All quadratic terms in the model have significance levels of P < 0.05, suggesting that there is a clear optimal region for this process. In contrast, the significance level of adhesive layer thickness is P > 0.05, so its influence on damping performance is not significant. However, since its quadratic term is significant, it cannot be completely neglected.

3.6. Response Surface Analysis for First-Order Damping Loss Factor

Considering the interactive effects of different parameter combinations on the damping of the shaft, response surface plots were fitted for the above damping loss factor prediction model using Design-Expert software, as shown in **Figures 9-14**.

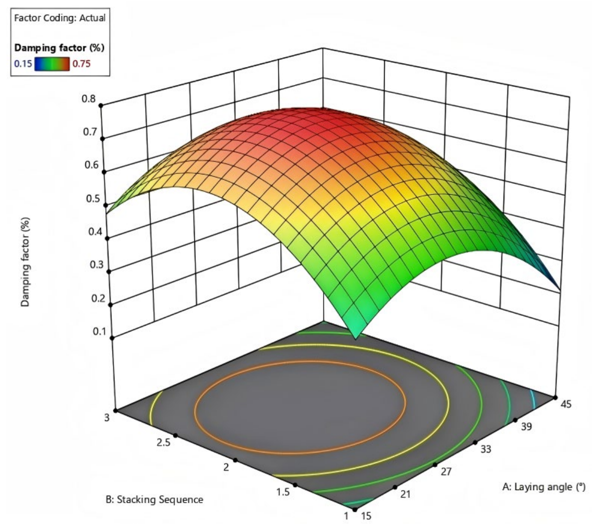

Figure 9. Box-Behnken experimental design plan.

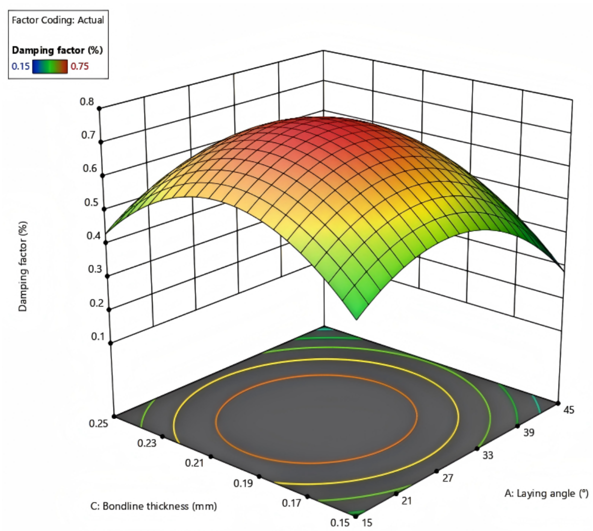

Figure 10. Interactive effect of ply angle and adhesive layer thickness.

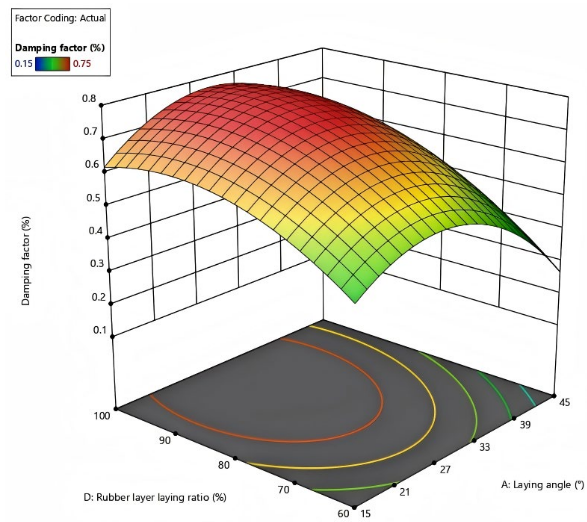

Figure 11. Interactive effect of ply angle and adhesive lay-up ratio.

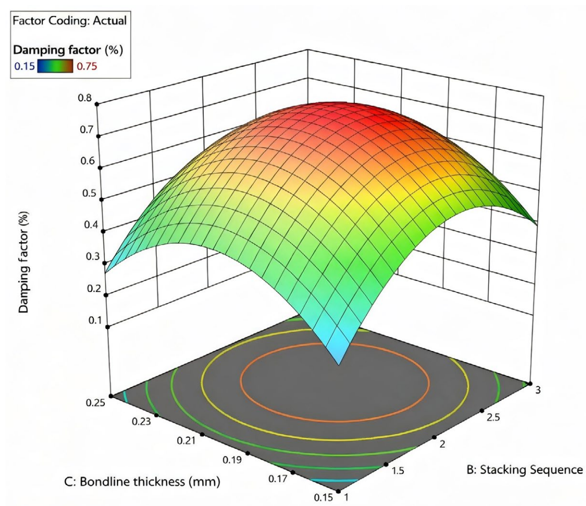

Figure 12. Interactive effect of stacking sequence and adhesive lay-up ratio.

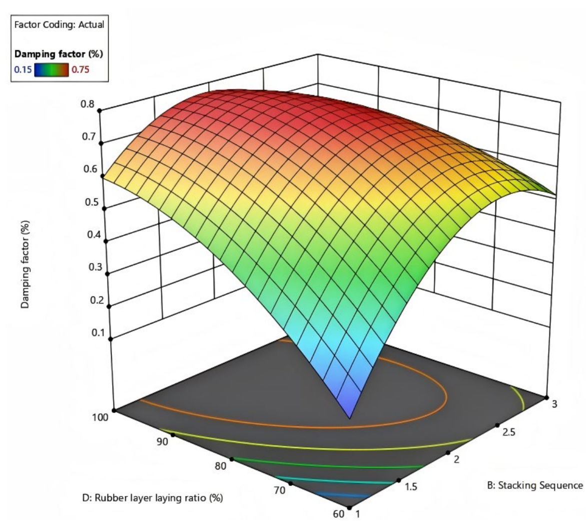

Figure 13. Interactive effect of stacking sequence and adhesive lay-up ratio.

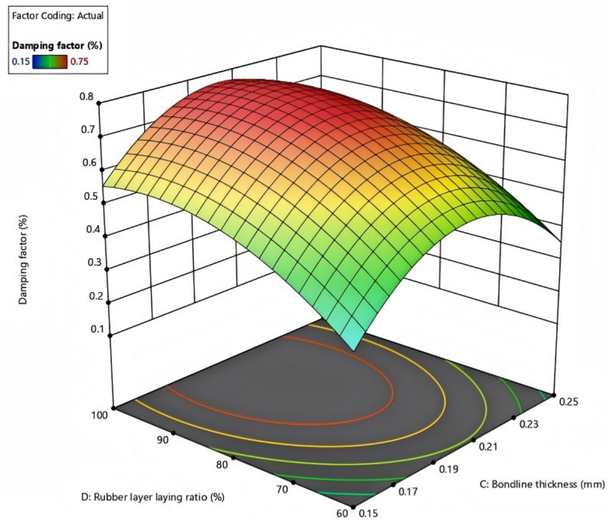

Figure 14. Interactive effect of adhesive layer thickness and adhesive lay-up ratio.

According to the above figures, it can be concluded that the damping loss factor first increases and then decreases with the increase of ply angle, shows a similar trend with the increase of adhesive layer thickness, and first increases and then decreases with the decrease of adhesive lay-up ratio with a relatively gentle initial trend. The damping loss factor is optimal when the ply angle is 21˚ - 33˚, the stacking sequence is symmetric, the adhesive layer thickness is 0.19 mm - 0.23 mm, and the adhesive lay-up ratio is 80% - 100%, corresponding to better damping performance of the shaft.

3.7. Establishment of First-Order Natural Frequency Prediction Model

Based on the experimental data of the first-order natural frequency in **Table 6**, multiple regression analysis was carried out using Design-Expert software, and the prediction model of the first-order natural frequency is obtained as follows:

$$\begin{aligned} f = {} & 969.44925 - 6.581 z_1 - 24.90167 z_2 - 41.61667 z_3 - 0.024417 z_4 \\ & + 1.15033 z_1 z_2 + 0.15 z_1 z_3 + 0.000917 z_1 z_4 - z_2 z_3 - 0.002 z_2 z_4 + 0.245 z_3 z_4 \end{aligned} \tag{17}$$

where: z_1, z_2, z_3 and z_4 represent the ply angle, stacking sequence, adhesive layer thickness and adhesive lay-up ratio, respectively.

3.8. Regression Diagnostics of the First-Order Natural Frequency Prediction Model

Table 8 shows the analysis of variance for the prediction model of the first-order natural frequency of the shaft.

As can be seen from **Table 8**, the P-value of the model is much less than 0.05, indicating that the model is extremely significant and has strong prediction ability. Among them, the significance levels of ply angle and stacking sequence are P < 0.01, so they have significant effects on the first-order natural frequency. In the parameter interactions, the significance level of the interaction between ply angle and stacking sequence is P = 0.0002 < 0.05, indicating that this interaction term has a significant influence on the first-order natural frequency.

Table 8. ANOVA of the prediction model for damping loss factor.

Source	Sum of Squares	Degrees of Freedom	Mean Square	F-value	P-value
Model	0.0802	10	0.008	86.86	<0.0001
z_1 : Ply angle	0.0764	1	0.0420	826.84	<0.0001
z_2 : Stacking sequence	0.0018	1	0.0675	19.36	0.0003
z_3 : Adhesive layer thickness	0.0000	1	0.0000	0.1996	0.6604
z_4 : Adhesive lay-up ratio	0.0000	1	0.0000	0.1986	0.6612
z_1z_2	0.0020	1	0.0020	22.00	0.0002
z_1z_3	4.800E−09	1	4.800E−09	0.0001	0.9943
z_1z_4	8.491E−07	1	8.491E−07	0.0092	0.9247
z_2z_3	8.891E−09	1	8.891E−09	0.0001	0.9923
z_2z_4	1.747E−08	1	1.747E−08	0.0002	0.9892
z_3z_4	3.928E−07	1	3.928E−07	0.0043	0.9487
Residual	0.0017	18	0.0001	—	——
Lack of Fit	0.0017	14	0.0001	—	—
Error	0.0000	4	0.0000	—	—
Total	0.0819	28	—	—	—

3.9. Response Surface Analysis of First-Order Natural Frequency

The response surfaces were fitted based on the above first-order natural frequency prediction model, as shown in Figures 15-17.

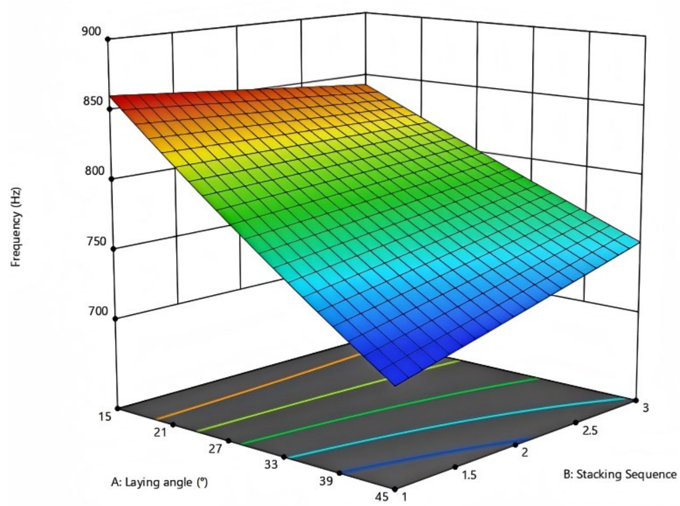

Figure 15. Interactive effect of ply angle and stacking sequence.

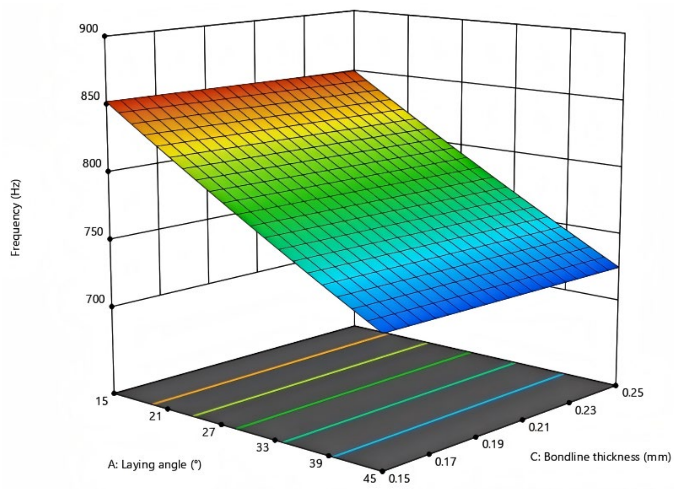

Figure 16. Interactive effect of ply angle and adhesive layer thickness.

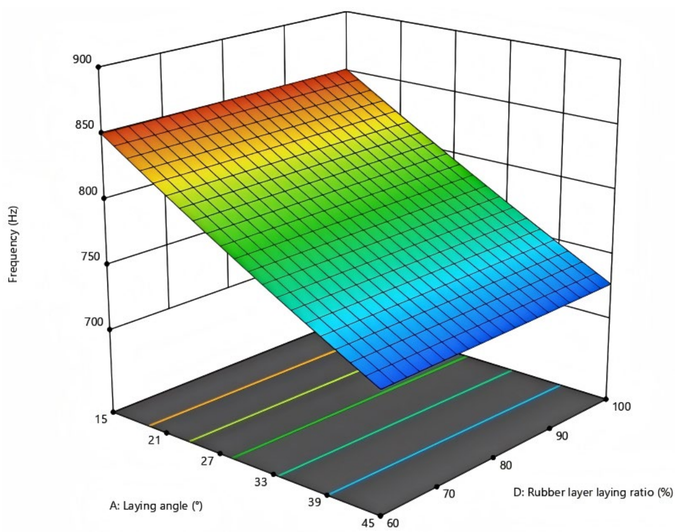

Figure 17. Interactive effect of ply angle and adhesive lay-up ratio.

As can be seen from the above figures, the first-order modal frequency decreases linearly with the increase of ply angle, while adhesive layer thickness and adhesive lay-up ratio have little effect on the first-order modal frequency.

4. Optimization of Lay-Up Structure and Bonding Surface Structure Based on Genetic Algorithm

Aiming at the parameter optimization of lay-up and adhesive layers for Al/CFRP shafts, the damping loss factor and the first-order natural frequency are mutually constrained, making it difficult to achieve a good balance between the two properties. Therefore, selecting an appropriate weighting factor is beneficial to improving its overall performance and minimizing its negative effects. Considering the above requirements, the Genetic Algorithm [18] is adopted for optimization, and the Technique for Order Preference by Similarity to an Ideal Solution (TOPSIS) is used for further selection.

The specific steps of parameter screening using the TOPSIS method are as follows: firstly, standardize the initial data to establish a normalized decision matrix; then perform weighting operations on the matrix, where both the damping loss factor and the first-order natural frequency are assigned a weight coefficient of 0.5. Subsequently, the positive ideal solution and negative ideal solution of each evaluation index are determined, and the Euclidean distances between each alternative and the positive/negative ideal solutions are calculated. Finally, the alternatives are ranked according to the relative closeness, and the parameter combination with the maximum relative closeness is determined as the optimal solution.

The Genetic Algorithm is programmed and solved using MATLAB software. The population size is set to 200, the maximum generation to 500, and the crossover rate to 0.7. The iterative optimization is realized by calling the objective function subroutine through the GA program. Figure 18 shows the distribution of optimal solutions, and Table 9 presents part of the multi-objective parameter optimization schemes for the Al/CFRP shaft.

According to the above results, $z_1 = 23.96$, $z_2 = 2$, $z_3 = 0.198$, $z_4 = 91.426$ is the most ideal combination. However, in the practical fabrication process of composite materials, all parameters are constrained by manufacturing conditions including manual glue application, fixture positioning limitation and adhesive fluidity, so high-precision quantitative control cannot be realized. Therefore, this parameter set is rounded to $z_1 = 24$, $z_2 = 2$, $z_3 = 0.2$, $z_4 = 90$. This parameter combination is selected as the optimal design scheme and this parameter combination is selected as the fabrication scheme for subsequent test specimens.

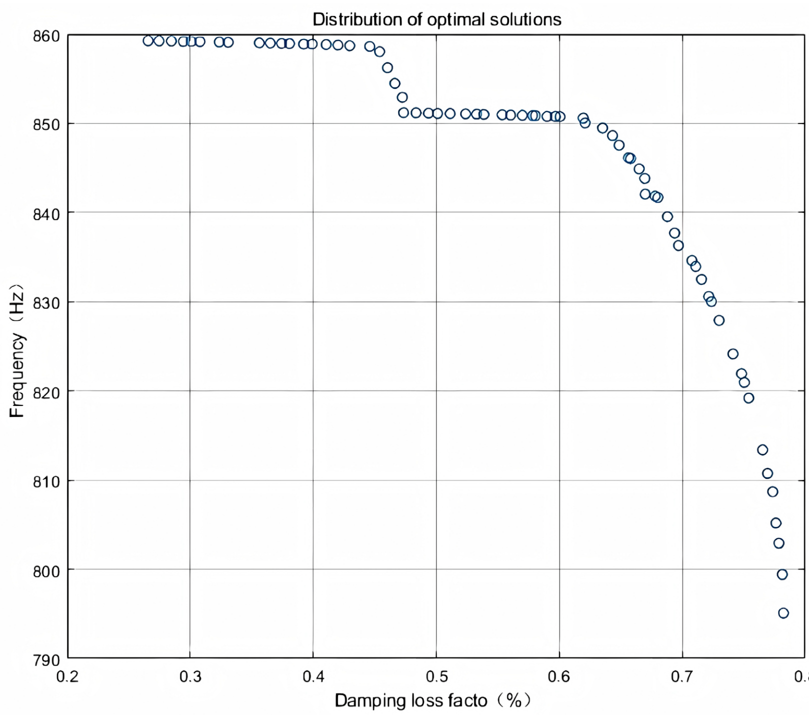

Figure 18. Distribution of optimal solutions.

Table 9. Optimal solution set.

No.	Ply angle/°	Stacking sequence	Adhesive layer thickness/mm	Adhesive lay-up ratio/%	Damping loss factor/%	First-order natural frequency/Hz	Relative closeness
1	23.96	2	0.198	91.426	0.767	812.991	0.9338
2	24.80	2	0.199	91.551	0.772	809.524	0.9336
3	23.24	2	0.200	91.862	0.762	815.999	0.9320
4	25.93	2	0.200	91.447	0.778	804.761	0.9306
5	26.58	2	0.201	93.046	0.779	802.113	0.9279
6	22.91	2	0.196	92.526	0.757	817.458	0.9275
7	26.90	2	0.202	91.172	0.781	800.676	0.9266
				…			
70	15.02	1	0.153	98.1	0.275	859.25	0.0814

5. Experimental Study on Shaft Vibration Performance

5.1. Specimen Preparation

According to the optimization results presented above, aluminum alloy/carbon fiber (Al/CFRP) shaft specimens were fabricated. The main manufacturing process of the Al/CFRP shaft specimen includes preparation and surface treatment of the aluminum alloy core, preparation and coating of the adhesive layer, cutting and laying of carbon fiber prepreg, high-temperature curing, and post-processing. The finished specimen is shown in Figure 19.

(a) Aluminum alloy shaft.

(b) Al/CFRP shaft.

Figure 19. Physical photograph of the specimen.

5.2. Construction of the Experimental Platform

According to the actual construction of the experimental platform for modal analysis of the specimen in this paper, the setup is shown in Figure 20. The impact hammer method is adopted for pulse excitation. The fixing method of the specimen is shown in **Figure 21**. In the measurement system, the model of the force sensor is 2302-10, which is mounted on the impact hammer. The model of the triaxial accelerometer is 356A25. Seven measuring points are arranged on the shaft surface, as shown in **Figure 22**. The seven measuring points are divided into four groups for testing: the first three groups measure two points each, and the last group measures the middle single point.

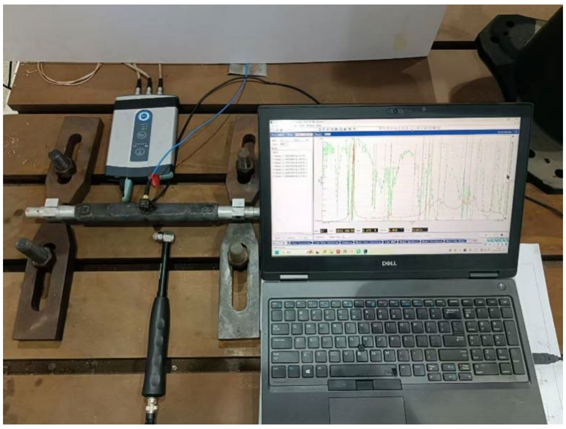

Figure 20. Modal test platform.

Figure 21. Fixing method of the shaft.

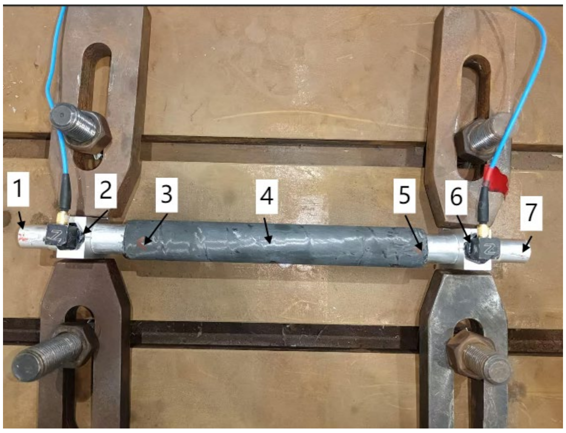

Figure 22. Distribution of measuring points.

5.3. Result Comparison and Analysis

Finite element analysis and modal test analysis were carried out respectively for the Al/CFRP shaft and the aluminum alloy shaft. The first four natural frequencies and damping loss factors obtained are shown in Table 10 and Table 11.

Table 10. Simulation and experimental data of the first 4 natural frequencies.

Order	Aluminum alloy shaft		Al/CFRP shaft	
	Simulation Value (Hz)	Experimental Value (Hz)	Simulation Value (Hz)	Experimental Value (Hz)
1	758.1	731.95	816.83	788.24
2	1276.4	1223.8	1363.9	1310.71
3	2532.7	2389.1	2586.2	2469.82
4	3483.4	3247.2	3515.4	3331.54

Table 11. Simulation and experimental data of the first 4 damping loss factors.

Order	Aluminum alloy shaft		Al/CFRP shaft	
	Simulation Value (%)	Experimental Value (%)	Simulation Value (%)	Experimental Value (%)
1	0.2	0.18	0.72	0.69
2	0.2	0.18	0.41	0.38
3	0.2	0.18	0.34	0.33
4	0.2	0.18	0.23	0.19

It can be seen from the tables that some differences between simulation and experimental data are inevitable, which are caused by boundary conditions, material impurities, curing temperature of carbon fiber, and other factors. For the aluminum alloy shaft, the deviations of the first four natural frequencies between finite element simulation and experimental data are 3.45%, 4.12%, 5.67%, 6.78% in sequence, and the deviation of the first four damping loss factors is 10%. For the Al/CFRP shaft, the deviations of the first four natural frequencies between finite element simulation and experimental data are 2.8%, 2.5%, 3.6%, 4.8% in sequence, and the deviations of the first four damping loss factors are 4.17%, 7.32%, 2.94%, 17.39% in sequence. All deviations are within a reasonable range, indicating that the simulation model has high accuracy.

By comparing the experimental data of the aluminum alloy shaft and the Al/CFRP shaft, the first four natural frequencies of the Al/CFRP shaft are increased by 7.69%, 7.1%, 3.38%, and 2.6% in sequence compared with the aluminum alloy shaft, and the first four damping loss factors are increased by 283.3%, 111.1%, 83.3%, and 5.56% in sequence.

6. Conclusions

In this paper, a carbon fiber/aluminum alloy shaft is taken as the research object. Based on the response surface methodology, prediction models for the first-order damping loss factor and natural frequency of the shaft are fitted, and an optimal design scheme for the layup structure parameters and bonding surface structure parameters is proposed. The conclusions are as follows:

1) The damping loss factor first increases and then decreases with the increase of layup angle, shows a trend of first increasing and then decreasing with the increase of adhesive layer thickness, and first increases and then decreases with the decrease of adhesive layer coverage ratio. The first-order modal frequency decreases linearly with the increase of layup angle, while the adhesive layer thickness and coverage ratio have little effect on the first-order modal frequency.

2) A set of parameter combinations closest to the ideal solution (maximizing both the first-order natural frequency and damping loss factor) is obtained by genetic algorithm: layup angle of 24˚, symmetric layup, adhesive layer thickness of 0.2 mm, and adhesive layer coverage ratio of 90%.

3) According to the optimal design parameters obtained from multi-objective optimization, Al/CFRP shaft specimens were fabricated. Through modal test analysis, compared with the aluminum alloy shaft, the first-order modal frequency and damping loss factor of the optimized Al/CFRP shaft are increased by 7.69% and 283.30%, respectively, achieving better vibration damping performance.

Conflicts of Interest

The authors declare no conflicts of interest regarding the publication of this paper.

References

[1] Nie, J.F. (2016) Research on Structure and Dynamic Characteristics of Helicopter Drive Shaft System. Harbin University of Science and Technology. (In Chinese) https://kns.cnki.net/kcms2/article/abstract?v=nTS8fe6ew4r1XmS8kqs9qoQHPEbuOUuGo2gjJuan-nAk8BuIDFq1Dm_l3yah2LOY6UoGS2iuBUpF5NpmnyXlIf_tSiNE_k_Li7Kb8-z4pYNqZXkvyCSZtdx7D-hT5BQGldHQAzEF2p94dRDMSZu-vP5DamjHVyAFIB-GPKCElOgHA7MUoOIqjPwZ-bXoI_GWfa&uniplatform=NZKPT&language=CHS

[2] Xie, B.L., Zhang, M., Zhou, M.G., *et al.* (2018) Dynamic Characteristic Analysis and Vibration Reduction Design of Automobile Drive Shaft. *Machinery Design & Manufacture*, **6**, 63-65. (In Chinese) https://doi.org/10.19356/j.cnki.1001-3997.2018.06.017

[3] Zhong, Z.F., Nie, P. and Lu, J. (2016) Research on Automobile Drive Shaft Based on Finite Element Method. *Journal of Mechanical Transmission*, **40**, 155-157. (In Chinese) https://doi.org/10.16578/j.issn.1004.2539.2016.06.034

[4] Kim, W., Argento, A. and Mohanty, P.S. (2004) Bending Natural Frequencies of Circular CFRP Shafts with a Metal Core or Casing. *Journal of Composite Materials*, **38**, 475-494. https://doi.org/10.1177/0021998304040560

[5] Gubran, H.B.H. and Gupta, K. (2004) The Effect of Stacking Sequence and Coupling Mechanisms on the Natural Frequencies of Composite Shafts. *Journal of Sound and Vibration*, **282**, 231-248. https://doi.org/10.1016/j.jsv.2004.02.022

[6] Sino, R., Baranger, T.N., Chatelet, E. and Jacquet, G. (2007) Dynamic Analysis of a Rotating Composite Shaft. *Composites Science and Technology*, **68**, 337-345. https://doi.org/10.1016/j.compscitech.2007.06.019

[7] Mutasher, S.A. (2008) Prediction of the Torsional Strength of the Hybrid Aluminum/Composite Drive Shaft. *Materials & Design*, **30**, 215-220.

https://doi.org/10.1016/j.matdes.2008.05.024

[8] Sarvestani, Y.H., Hoa, V.S. and Hojjati, M. (2016) Effects of Shear Loading on Stress Distributions at Sections in Thick Composite Tubes. *Composite Structures*, **140**, 433-445. https://doi.org/10.1016/j.compstruct.2015.12.067

[9] Xu, Z.T. and Zhu, R.P. (2006) Primary Resonance Analysis of Composite Drive Shaft for Helicopter. *Journal of Mechanical Engineering*, **42**, 155-160. (In Chinese) https://kns.cnki.net/kcms2/article/abstract?v=nTS8fe6ew4rLNoB-ngWQ7pDPPTApvxE9SvUrP8dDvWg6XTyBx8PJWY6f8K-41I6or-DexX6bryiN6Y9MQShuc90dzbG9PZhPuieO-hPEH5B46p_21ODghGh0YFI18sD9TaMwIqIvkZUn3VPgwlX-isNqhmg-FQW8EhJcEpsJQn9xEUCwBLOZkDfXg==&uniplatform=NZKPT&language=CHS

[10] Sun, G., Yu, H., Wang, Z., Xiao, Z. and Li, Q. (2018) Energy Absorption Mechanics and Design Optimization of CFRP/Aluminium Hybrid Structures for Transverse Loading. *International Journal of Mechanical Sciences*, **150**, 767-783. https://doi.org/10.1016/j.ijmecsci.2018.10.043

[11] Kabir, M.H., Fawzia, S., Chan, T.H.T., Gamage, J.C.P.H. and Bai, J.B. (2016) Experimental and Numerical Investigation of the Behaviour of CFRP Strengthened CHS Beams Subjected to Bending. *Engineering Structures*, **113**, 160-173. https://doi.org/10.1016/j.engstruct.2016.01.047

[12] Shao, J.R., Liu, N., Yang, Y., *et al.* (2023) Study on Bonding Characteristics and Failure Law of CFRP Composite Components. *Chinese Journal of Applied Mechanics*, **40**, 1058-1067. (In Chinese) https://kns.cnki.net/kcms2/article/abstract?v=nTS8fe6ew4ptBbcge4WA023mVwpxr6c64Ncfr-qR5eo3vYgstWL-SaEMP3qZwgDkA2ZifytHSa4iBiTfkwyVfU1o28e10EIzG7HwLgy52UmwF_1II8X-Thi0_qnNDyBwFtjcXq5SvB3bXjipY1dg7T1Y_DlmhLAoN3-GSf_JsmUchp_XHcK-9YQvGAmArRO7&uniplatform=NZKPT&language=CHS

[13] Ramezani, F., Simões, B.D., Carbas, R.J.C., Marques, E.A.S. and da Silva, L.F.M. (2023) Developments in Laminate Modification of Adhesively Bonded Composite Joints. *Materials*, **16**, Article 568. https://doi.org/10.3390/ma16020568

[14] Kupski, J., Teixeira de Freitas, S., Zarouchas, D., Camanho, P.P. and Benedictus, R. (2019) Composite Layup Effect on the Failure Mechanism of Single Lap Bonded Joints. *Composite Structures*, **217**, 14-26. https://doi.org/10.1016/j.compstruct.2019.02.093

[15] Pisharody, A. and Smith, D.E. (2022) An Experimental and Numerical Investigation into the Effects of Bond Line Thickness Variations on the Strength of Composite Bonded Joints. *Composite Structures*, **279**, Article 114789. https://doi.org/10.1016/j.compstruct.2021.114789

[16] Jing, S.W. (2022) Study on Damping Characteristics of Metal/Carbon Fiber Composite Hybrid Structures. Xi'an University of Architecture and Technology. (In Chinese) https://doi.org/10.27393/d.cnki.gxazu.2022.000405

[17] Izamshah, R., Zuraidah, Z., Kasim, M.S., Hadzley, M. and Amran, M. (2015) Multi Objective Optimization of Cutting Parameters in Machining Cellulose Based Hybrid Composites. *Applied Mechanics and Materials*, **761**, 287-292. https://doi.org/10.4028/www.scientific.net/amm.761.287

[18] Li, Y. (2019) Design and Multi-Objective Quality Matching Optimization of Key Structural Components of Machining Center Based on Composite Materials. Lanzhou University of Technology. (In Chinese) https://kns.cnki.net/kcms2/article/abstract?v=nTS8fe6ew4oU-

haJA8Z2Nxa6lhpbA1ljtHWGDqDS2PrZF-q4vp5YicDxj-
jAb4SoGXaV3aYeRWB50WKkamKmXc0ZilsCGL5-pbeFXJaZcY-
buGVoMuoXJrstPUEcYzLz10uvHipOF9Mu7Bbd6V9hPIq-
BDqnGpSyIPuYKbzCrRy0ysxPW4Wg7pqhGQ==&uniplatform=NZKPT&lan-
guage=CHS